CO Reduction Hot Paper

How to cite: *Angew. Chem. Int. Ed.* **2021**, *60*, 11133–11137
International Edition: doi.org/10.1002/anie.202016332
German Edition: doi.org/10.1002/ange.202016332

Hidden Mechanism Behind the Roughness-Enhanced Selectivity of Carbon Monoxide Electrocatalytic Reduction

Yinghuan Liu, Huijun Jiang, and Zhonghuai Hou**

Abstract: *High roughness has been proved to be an effective design strategy for electrocatalyst in many systems. Especially, high selectivity of carbon monoxide reduction (CORR) in competition with the hydrogen evolution reaction has been observed on high roughness electrocatalysts. However, the two well-known mechanisms, i.e., decreasing the energy barrier of CORR and increasing local pH, failed to understand the roughness-enhanced selectivity in a recent experiment. Herein we unravel the hidden mechanism by establishing a comprehensive kinetic model for CORR on catalysts with different roughness factors. We conclude that the roughness-enhanced CORR selectivity is actually kinetic controlled by local-electric-field-directed mass transfer of adsorbed species on the electrode surface. Several ways to optimize CORR selectivity are predicted. Our work highlights the kinetics in electrocatalysis on nanocatalysts, and provides a conceptually new principle for future catalyst design.*

Converting CO_2 into value-added multi-carbon feedstock by electrochemical reactions is considered to be a promising way of mitigating the growing energy demands and reducing CO_2 in the atmosphere.[1–7] CO_2 reduction reaction consists of a $2e^-$ process from CO_2 to CO and a following surface reaction from CO to multi-carbon products.[8–10] As the CO_2 to CO process has been well established, unraveling the mechanism underlying CO reduction reaction (CORR) with high selectivity is then of particular importance.[11–15] Nevertheless, as the equilibrium potential of CORR is close to that of hydrogen evolution reaction (HER), elevation of CORR activity is inevitably accompanied by the unwanted promotion of HER activity.[8,16] So far, there are two major proposed mechanisms to enhance CORR selectivity, i.e., increasing solely the intrinsic activity of CORR[17–19] or increasing local pH to suppress HER activity.[1,16,20–22]

Recently, an effective design strategy of simply increasing the roughness factor (RF) of catalysts has been reported to improve the selectivity of CORR in experiments.[23–27] However, both the electrochemical-active-surface-area (ECSA) normalized CORR rate and the local pH near the electrode surface were found to keep nearly constant with increasing RF. The failure of both CORR-activity-promoting and local-pH-elevating mechanisms implies a new mechanism underlying the RF-enhanced CORR selectivity.[24] Unraveling this novel mechanism would provide insight into easy-taking design principles for catalysts with enhanced selectivity.

Here, we address the mechanistic issue by establishing a comprehensive reaction-diffusion model of CORR on multisite catalysts with constant local pH. Key kinetic processes are included, such as adsorption, desorption, surface reactions, diffusion, and specifically the directional mass transfer due to curvature-induced local electric field.[28,29] Simulations successfully reproduce the key experimental finding that catalysts with high RF (i.e., surface with large number of high curvature sites (HC sites)) would efficiently enhance the multi-carbon selectivity.[24] Detailed analysis shows that distribution of surface OH^- is redistributed by field-induced mass transfer, leading to high OH^- coverage at HC sites for high RF catalysts. HER activity is therefore suppressed and results in an enhanced CORR selectivity. In other words, the RF-induced high CORR performance is actually kinetic-controlled by directional field-induced mass transfer on the rough surface. Serval approaches are subsequently predicted to optimize the selectivity of carbon feedstock by modifying the kinetics.

To reveal the underlying mechanism, we employ a comprehensive reaction-diffusion model for enhanced CORR on multisite catalysts. The roughness in experiments is mimicked by HC sites randomly distributed on a planar electrode surface. As shown in Figure 1, adsorption, desorption, diffusion, reduction of CO, as well as the accompanied HER are included. Specially, since the curvature of HC sites on the electrode surface can lead to an enhanced local electric field, the local-field-induced directional mass transfer is also taken

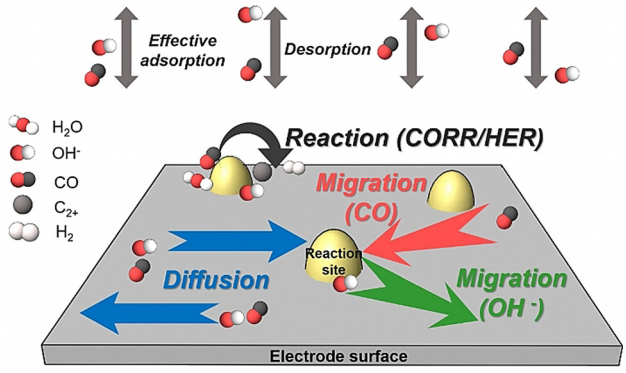

Figure 1. Schematic of the kinetic model for CORR and HER on roughness catalysts. Products of the main reaction CORR are hydrocarbons while the one for sub-reaction HER is hydrogen.

[*] Y. Liu, Dr. H. Jiang, Dr. Z. Hou
Department of Chemical Physics & Hefei National Laboratory for Physical Sciences at the Microscale, iChEM, University of Science and Technology of China
Hefei, Anhui 230026 (China)
E-mail: hjjiang3@ustc.edu.cn
hzhlj@ustc.edu.cn

Supporting information and the ORCID identification number(s) for the author(s) of this article can be found under: https://doi.org/10.1002/anie.202016332.

into account.[28–30] The reaction-diffusion equations (RDE) for CORR on multisite electrocatalysts surface are derived as follows (Details in supplementary information, SI) [Eqs. (1a)–(1b)].

$$\frac{\partial\theta^{CO}(r)}{\partial t} = k_{ad}^{CO}c_0^{CO}\left(1-\theta^{CO}(r)\right) - k_d{}^{CO}\theta^{CO}(r) + D^{CO}\nabla^2\theta^{CO}(r) - \frac{D^{CO}}{k_BT}\nabla\cdot\left[\theta^{CO}(r)\left(1-\theta^{CO}(r)\right)\nabla\left(\partial_{\theta^{CO}}V^{CO}(r)\right)\right] - k_{\eta=0}^{COR}\exp\left(\lambda^{COR}\eta^{COR}\right)\theta^{CO}(r) \tag{1a}$$

$$\frac{\partial\theta^{OH}(r)}{\partial t} = k_{ad}^{OH}c_0^{OH}\left(1-\theta^{OH}(r)\right) - k_d{}^{OH}\theta^{OH}(r) + D^{OH}\nabla^2\theta^{OH}(r) - \frac{D^{OH}}{k_BT}\nabla\cdot\left[\theta^{OH}(r)\left(1-\theta^{OH}(r)\right)\nabla\left(\partial_{\theta^{OH}}V^{OH}(r)\right)\right] + 4k_{\eta=0}^{COR}\exp\left(\lambda^{COR}\eta^{COR}\right)\theta^{CO}(r) + k_{\eta=0}^{HER}\left(1-\theta^{\boldsymbol{OH}}(r)\right)\exp\left(\lambda^{HER}\eta^{HER}\right) \tag{1b}$$

In the RDEs, variables with superscript OH, CO, or H_2O denote the corresponding ones for species OH^-, CO, or H_2O, respectively. $\theta(r)$ is the surface coverage of each chemical species at location r.

In the right side of Equation (1a) and (1b), the first-(second) term describes the adsorption(desorption) of CO and OH^- respectively, where $k_{ad}(k_d)$ is the adsorption(desorption) rate constant. In the first term, c_0 is the concentration in solution near the electrode surface, and $1-\theta(r)$ measures the number of available space for adsorption. Here, the effect of local pH is taken into account by the relationship $pH = -\log(10^{-14}/c_0^{OH})$. As experiments demonstrated that local pH keeps nearly unchanged for CORR on catalysts with different RF, c_0^{OH} is set to be constant.[24] Similarly, c_0^{CO} is also set to be constant due to the constant CO flow in experiments.[24] The second term describes the desorption with constants k_d.

The third and fourth terms describe the mass transfer on the electrode surface due to normal diffusion with diffusion constant D and curvature-enhanced local electric field,[28,29] respectively. Here, k_B is the Boltzmann constant and T the temperature. The effective interaction potential between local electric field and chemical species is chosen as Gaussian-like $V(r) = \sum_{site}\alpha\theta u_0 exp(-|r-r_{site}|^2/(r_0^2))$,[28] where α is the interaction strength, u_0 denotes the intensity of electric field on an isolated single HC site located at r_{site}, and r_0 is the characteristic length.[28,30] Since CO can be polarized by the local electric field and be attracted to HC sites, we take $\alpha_{CO}<0$ to describe such attraction. On the contrary, the adsorbed OH^- would be pushed away from HC sites, and consequently $\alpha_{OH}>0$.

The fifth term shows the change of θ due to the main reaction CORR basing on Butler-Volmer equation, where $k_{\eta=0}^{COR}$ is the reaction rate constant at the equilibrium potential, η^{COR} is the overpotential, and λ^{COR} denotes the reducing coefficient of the energy barrier by the applied overpotential.[8] Additionally, the last term in Equation (1b) describes the change of OH^- coverage as a result of the side reaction HER, where $k_{\eta=0}^{HER}$, η^{HER} and λ^{HER} are the rate constant at equilibrium potential, the overpotential and the reducing coefficient for HER, respectively.[31,32] It has been acknowledged that for HER in alkaline conditions, OH^- would adsorb on the electrode surface and further blocks the HC sites for the dissociation of water and then suppresses the HER.[31] The effect of competition between adsorption of OH^- and dissociation of water in HER is taken into account by $1-\theta^{OH}$ which measures the remained space for water dissociation.[32,33] As the reaction rates also depend on the local electric potential which is highly enhanced on HC sites, the range of grids on which reactions happen should be truncated around HC sites. Accordingly, the reactions are considered to occur only on HC sites.

In simulations, Equation (1) is discretized on a $L\times L$ rectangle lattice with $n\times n$ grids and is solved by Euler difference methods with periodic boundary conditions. N HC sites (proportional to the experimentally measured roughness factor RF) are randomly distributed on the surface. Parameters are normalized by D_{OH^-}, L and k_BT. The apparent rates ν_{CORR} and ν_{HER} for CORR and HER are summations over the total electrode surface. The Faradaic efficiency (FE) can be calculated by $e = \langle(4\nu_{CORR})/(4\nu_{CORR}+\nu_{HER})\rangle$, and the ECSA-normalized rates are $\tilde{\nu}_{HER(CORR)} = \langle\nu_{HER(CORR)}/N\rangle$ where $\langle\cdot\rangle$ denotes ensemble average over different distribution of HC sites with the same N.

CORR on multisite catalysts is simulated with parameters listed in Table S1 (Determination of the parameters are discussed in SI). To validate our theoretical model, FE of the main product hydrocarbons (blue bar) and the side product H_2 (grey bar) for different RF are plotted in Figure 2(a). As N increases, FE of hydrocarbons increases while FE for H_2 decreases. This leads to an enhanced selectivity of hydrocarbons from less than 40% at $N=5$ to more than 80% at $N=40$. The simulated selectivity (dash line) and that in experiments[24] (red star) are compared in the inset of Figure 2(a). It can be observed that the RF-enhanced selectivity in experiments[24] is well reproduced by our simulations. For further validation, apparent rates of CORR and HER are also calculated in our simulations. Similar to that in the experiments,[24] ν_{CORR} (blue line) increases significantly with RF, while ν_{HER} (gray line) changes slightly as shown in the top panel in Figure 2(b), leading to the observed enhancement of CORR selectivity.

The intrinsic activities for CORR and HER are explored by ECSA-normalized reaction rate $\tilde{\nu}_{HER(CORR)}$ which are presented in the bottom of Figure 2(b). It can be found that $\tilde{\nu}_{CORR}$ diminutively changes with N, which indicates a nearly unchanged CORR intrinsic activity. Nevertheless, $\tilde{\nu}_{HER}$ and consequently the intrinsic activity of HER declines sharply with increasing N. The above observations agree with experimental ones well, implying that the CORR-activity-promoting mechanism fails to explain the enhanced CORR selectivity on multisite catalysts. Furthermore, as experimental observations demonstrated that local pH keeps nearly unchanged for CORR on catalysts with different RF, the concentration of OH^- in the solution near the electrode surface c_0^{OH} is set to be constant (Figure 2(c)). This rules out the local-pH-elevating mechanism from the enhanced CORR selectivity. One may argue that local PH may not be the OH^-

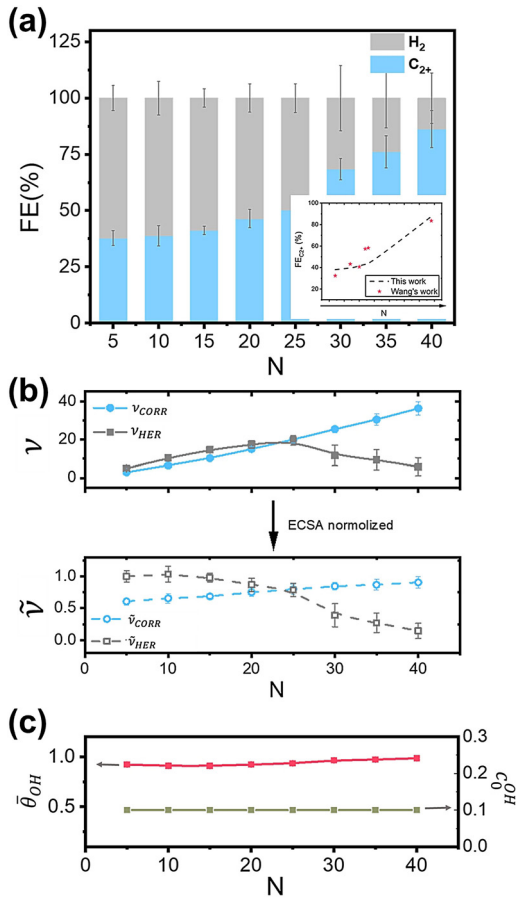

Figure 2. Selectivity and activity of CORR on roughness catalysts. (a) The simulated results of Faradic efficiency (FE) of hydrocarbons (HC) and hydrogen (H_2). The inset shows our simulation results and those in experiments in Ref. [24] (b) Dependence of the apparent rates ν (top) and ECSA-normalized rates $\tilde{\nu}$ (bottom) for CORR and HER on the sites number *N*. (c) The averaged OH^- coverage on the electrode surface (red line) and the OH^- concentration near the electrode surface (green line) of catalysts with different roughness factors.

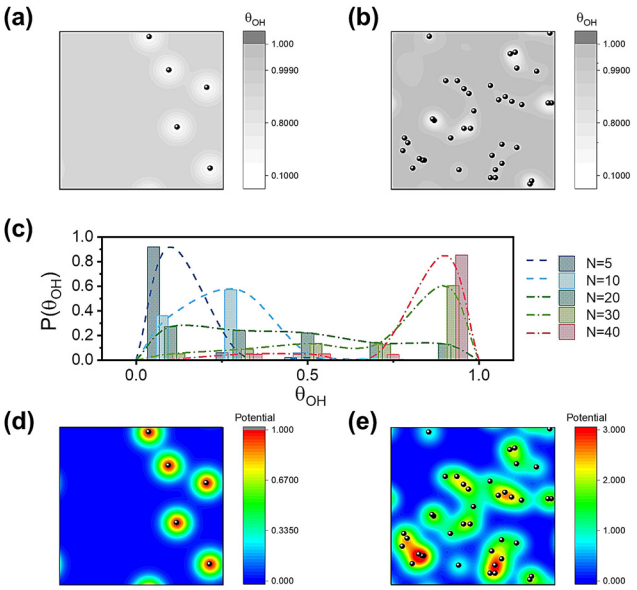

Figure 3. Mechanism of RF enhanced CORR selectivity. (a) and (b) are the surface coverage of OH^- on the catalysts with $N=5$ and $N=40$, respectively, in which the black particles are the location of HC sites. (c) is the distribution of OH groups on the HC sites of catalysts with different roughness with the interaction strength 10.0. (d) and (e) are potential of OH groups in the electric field induced by catalysts with $N=5$ and $N=40$, respectively.

concentration in the solution near the electrode surface but OH^- coverage on the electrode surface. Thus, the averaged coverage of OH^-, $\bar{\theta}_{OH}$, on the electrode surface is also plotted in Figure 2(c). Clearly, $\bar{\theta}_{OH}$ is also nearly unchanged when the RF increases, demonstrating again that local-pH-elevating mechanism is not the reason for enhanced selectivity for CORR on multisite catalysts.

To investigate the very reason for the observed HER suppression on multisite catalysts, we now focus on adsorbed OH^- on the electrode surface during the electrocatalytic process. Snapshots of stationary OH^- surface coverages, θ_{OH}, on the catalysts with different N are shown in Figure 3(a) and Figure 3(b). For low roughness catalysts, there are several low coverage regions (white area in Figure 3(a)) and all of the HC sites (black particles in Figure 3(a)) are located in the center of these regions. Remarkably, for high roughness catalysts, only few of the HC sites locate in the low coverage area and most of them locate in relatively high coverage area (Figure 3(b)). To quantitatively compare the observed difference, the probability distribution of HC sites with given θ_{OH} is plotted in Figure 3(c). For small RF catalysts (such as $N=5$,10, blue bars in Figure 3(c)), the distribution is Gaussian-like with a peak of low coverage. As the RF increases to be medium (such as $N=20$,30, green bars in Figure 3(c)), a new peak of high coverage emerges, and the distribution changes to be bimodal. The peak of low coverage then declines with further increased RF (such as $N=40$, red bar in Figure 3(c)), while the peak of high coverage rises gradually. Since the reaction rates of HER would decrease as the HC sites are blocked by OH^-, the high-RF-induced high coverage of OH^- on HC sites thus contributes to the suppression of HER in the electrocatalytic process.

Now, the key point turns to why the coverage of OH^- on HC sites is low for low RF catalysts and increases as RF increases. As OH^- is generated at the HC sites and can diffuse to nearby area by normal diffusion according to the concentration gradient, the coverage of OH^- would be higher on HC sites than other regions of the surface (or nearly equal if diffusion is much faster than reactions). As mentioned in the kinetic modeling part, the curvature-enhanced local electric field can also lead to an extra mass transfer besides the normal diffusion. The interaction potentials between local electric field and OH^- on the surface of electrode with low ($N=5$) and high ($N=40$) RF are plotted in Figure 3(d,e), respectively. It is observed that, low RF catalyst leads to separated high potential islands located around each HC site, resulting in directional mass transfer of OH^- from HC sites to other regions of the electrode surface. Such mass transfer then leads to the concentration distribution shown in Figure 3(a) where OH^- coverage is low around HC sites, i.e., OH^-

coverage at HC sites is depressed by the local-field-induced mass transfer.

However, as shown in Figure 3(e), the islands of high interaction potential around HC sites are overlapped for high RF catalysts. Consequently, there are some closely approached HC sites located in regions of high interaction potential, while others have to distribute in regions of low potential. As the local-field-induced mass transfer is always from regions of the high interaction potential to ones with low potential, the depression of OH^- coverage is then weakened, and OH^- coverage at some HC sites increases as the concentration distribution presented in Figure 3(b). In short, the HER activity on high RF catalysts is suppressed by local-field-induced directional mass transfer of OH^-.

Based on the above revealed kinetic-controlled mechanism of multi-site enhanced high selectivity of CORR, it is possible to further improve the selectivity of carbon products by tuning kinetic factors.

One of the most significant kinetic factors is the interaction strength α between the local electric field and chemical species. Large α leads to high local-field-induced mass transfer while small α results in a weak one. As shown in Figure 4(a), CORR selectivity increases with the relative interaction strength α_{CO}/α_{OH} and saturates at large enough α_{CO}/α_{OH} for all of the catalysts with RF ranging from $N=5$ to 40. Interestingly, the saturated selectivity would reach to nearly 100% for catalysts with large RF at a lower relative interaction strength α_{CO}/α_{OH} in comparison with that for catalysts with small RF. The above findings indicate that the CORR selectivity can be well tuned in experiments by ways of increasing the ability of CO interacting with local electric field in relative to that of OH^-. For example, there may be some anions acting as Lewis acid and would interact with the Lewis base, CO, and then enhance the mass transfer within local electric field.[29,34,35]

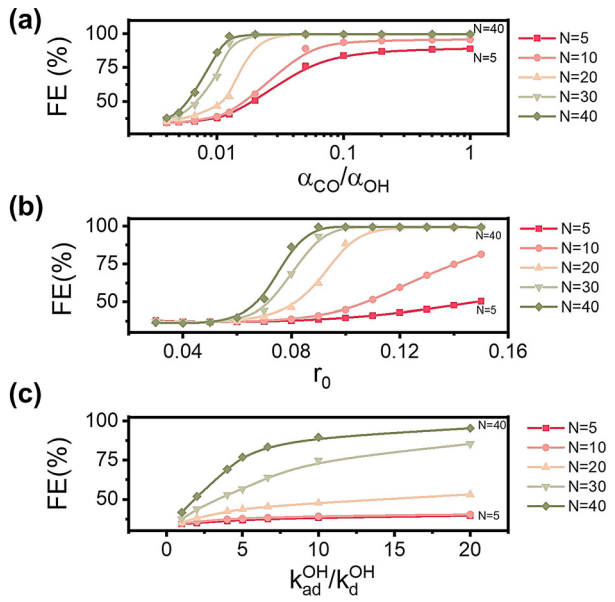

Figure 4. Prediction of the optimal CORR selectivity with optimized kinetic factors. (a) FE (selectivity) of CORR on catalysts with different roughness with the increasing interaction strength between adsorbed OH^- and local electric field. (b) The FE of HC products on catalysts with different roughness with the increasing characteristic length of electric field r_0. (c) the FE with the increasing equilibrium of adsorption and desorption of OH from bulk to the electrode surface.

The characteristic length of the local electric field is another significant kinetic factor for CORR selectivity. As shown in Figure 4(b), increasing the characteristic length r_0 can also enhance the CORR selectivity for all of the catalysts with different RF. The CORR selectivity on high RF catalyst is enlarged obviously as r_0 increases, while that on low RF catalysts increases slightly with increasing r_0. For large enough r_0 and RF, CORR selectivity reaches nearly 100%. As shown in FigureS(3), large r_0 prefers to form overlapped islands of high interaction potential and enhances the suppression of HER activity, while the activity of CORR changes little. As it is well known that modifying the ion strength of the electrolyte would manipulate the characteristic length efficiently,[36] CORR selectivity may be optimized by enlarging solely the characteristic length of the local electric field.

Besides the local electric field, the mass transfer is also controlled by the equilibrium of adsorption and desorption (k_{ad}^{OH}/k_d^{OH}) of OH^- from bulk to surface which determines the concentration of species on the electrode surface. It can be seen in Figure 4(c) that the selectivity of CORR is enhanced by an enlarged k_{ad}^{OH}/k_d^{OH}. For small k_{ad}^{OH}/k_d^{OH}, the selectivity is rather small and the difference of selectivity on catalysts with different RF is minor. As k_{ad}^{OH}/k_d^{OH} increases, the selectivity of CORR on high RF catalyst, such as $N=40$, is enhanced obviously (from 40% to nearly 100%) while that on low RF catalyst, such as $N=5$, shows little difference. This finding shows that for high RF catalysts, raising the ratio of k_{ad}^{OH}/k_d^{OH} would efficiently optimize the selectivity of CORR. However, optimizing the k_{ad}^{OH}/k_d^{OH} does little to the FE for catalysts with low RF.

In summary, a comprehensive kinetic model was employed to investigate CORR selectivity in competition with HER on catalysts of different roughness factors (RF). The kinetic model successfully reproduced the experimentally observed RF-enhanced CORR selectivity. It was revealed that the high-curvature-induced local electric field directs the mass transfer of OH^- during electrocatalytic process. High RF catalysts lead to a weaker local-field-induced mass transfer as a result of the highly overlapped local electric field. This further results in the suppression of HER and the enhancement of CORR selectivity. Based on the kinetic-controlled mechanism, several approaches were predicted to optimize CORR selectivity by modifying the kinetics of CORR and HER, such as the local-field-induced mass transfer, adsorption and desorption between bulk solution and electrode surface, etc. Our work highlights the kinetics in electrocatalysis on nanocatalysts, and provides a new principle for future catalyst design.

Acknowledgements

This work is supported by MOST (2018YFA0208702, 2016YFA0400904), NSFC (21973085, 21833007, 21790350, 21673212, 21521001), Anhui Initiative in Quantum Informa-

tion Technologies (AHY090200), and the Fundamental Research Funds for the Central Universities (WK2340000104).

Conflict of interest

The authors declare no conflict of interest.

Keywords: carbon monoxide reduction · kinetics · electrocatalysis · mechanistic studies · roughness

[1] Z. W. Seh, J. Kibsgaard, C. F. Dickens, I. Chorkendorff, J. K. Norskov, T. F. Jaramillo, *Science* **2017**, *355,* eaad4998.
[2] O. S. Bushuyev, P. De Luna, C. T. Dinh, L. Tao, G. Saur, J. van de Lagemaat, S. O. Kelley, E. H. Sargent, *Joule* **2018**, *2*, 825 – 832.
[3] S. Xu, E. A. Carter, *Chem. Rev.* **2019**, *119*, 6631 – 6669.
[4] D. D. Zhu, J. L. Liu, S. Z. Qiao, *Adv. Mater.* **2016**, *28*, 3423 – 3452.
[5] T. Zheng, K. Jiang, H. Wang, *Adv. Mater.* **2018**, *30*, 1802066.
[6] D. Gao, R. M. Arán-Ais, H. S. Jeon, B. Roldan Cuenya, *Nat. Catal.* **2019**, *2*, 198 – 210.
[7] M. B. Ross, P. De Luna, Y. Li, C.-T. Dinh, D. Kim, P. Yang, E. H. Sargent, *Nat. Catal.* **2019**, *2*, 648 – 658.
[8] Y. Hori, R. Takahashi, Y. Yoshinami, A. Murata, *J. Phys. Chem. B* **1997**, *101*, 7075 – 7081.
[9] J. Feng, S. Zeng, J. Feng, H. Dong, X. Zhang, *Chin. J. Chem.* **2018**, *36*, 961 – 970.
[10] A. Rendón-Calle, S. Builes, F. Calle-Vallejo, *Curr. Opin. Electrochem.* **2018**, *9*, 158 – 165.
[11] W. Luc, X. Fu, J. Shi, J.-J. Lv, M. Jouny, B. H. Ko, Y. Xu, Q. Tu, X. Hu, J. Wu, Q. Yue, Y. Liu, F. Jiao, Y. Kang, *Nat. Catal.* **2019**, *2*, 423 – 430.
[12] M. Jouny, W. Luc, F. Jiao, *Nat. Catal.* **2018**, *1*, 748 – 755.
[13] Y. Pang, J. Li, Z. Wang, C.-S. Tan, P.-L. Hsieh, T.-T. Zhuang, Z.-Q. Liang, C. Zou, X. Wang, P. De Luna, J. P. Edwards, Y. Xu, F. Li, C.-T. Dinh, M. Zhong, Y. Lou, D. Wu, L.-J. Chen, E. H. Sargent, D. Sinton, *Nat. Catal.* **2019**, *2*, 251 – 258.
[14] T.-T. Zhuang, Y. Pang, Z.-Q. Liang, Z. Wang, Y. Li, C.-S. Tan, J. Li, C. T. Dinh, P. De Luna, P.-L. Hsieh, T. Burdyny, H.-H. Li, M. Liu, Y. Wang, F. Li, A. Proppe, A. Johnston, D.-H. Nam, Z.-Y. Wu, Y.-R. Zheng, A. H. Ip, H. Tan, L.-J. Chen, S.-H. Yu, S. O. Kelley, D. Sinton, E. H. Sargent, *Nat. Catal.* **2018**, *1*, 946 – 951.
[15] J. Li, F. Che, Y. Pang, C. Zou, J. Y. Howe, T. Burdyny, J. P. Edwards, Y. Wang, F. Li, Z. Wang, P. De Luna, C. T. Dinh, T. T. Zhuang, M. I. Saidaminov, S. Cheng, T. Wu, Y. Z. Finfrock, L. Ma, S. H. Hsieh, Y. S. Liu, G. A. Botton, W. F. Pong, X. Du, J. Guo, T. K. Sham, E. H. Sargent, D. Sinton, *Nat. Commun.* **2018**, *9*, 4614.
[16] Y.-J. Zhang, V. Sethuraman, R. Michalsky, A. A. Peterson, *ACS Catal.* **2014**, *4*, 3742 – 3748.
[17] A. A. Peterson, J. K. Nørskov, *J. Phys. Chem. Lett.* **2012**, *3*, 251 – 258.
[18] C. W. Li, J. Ciston, M. W. Kanan, *Nature* **2014**, *508*, 504 – 507.
[19] S. H. Lee, I. Sullivan, D. M. Larson, G. Liu, F. M. Toma, C. Xiang, W. S. Drisdell, *ACS Catal.* **2020**, *10*, 8000 – 8011.
[20] M. Ma, B. J. Trzesniewski, J. Xie, W. A. Smith, *Angew. Chem. Int. Ed.* **2016**, *55*, 9748 – 9752; *Angew. Chem.* **2016**, *128*, 9900 – 9904.
[21] R. Kas, R. Kortlever, H. Yılmaz, M. T. M. Koper, G. Mul, *ChemElectroChem* **2015**, *2*, 354 – 358.
[22] X. Wang, C. Xu, M. Jaroniec, Y. Zheng, S. Z. Qiao, *Nat. Commun.* **2019**, *10*, 4876.
[23] B. A. Zhang, T. Ozel, J. S. Elias, C. Costentin, D. G. Nocera, *ACS Cent. Sci.* **2019**, *5*, 1097 – 1105.
[24] L. Wang, S. Nitopi, A. B. Wong, J. L. Snider, A. C. Nielander, C. G. Morales-Guio, M. Orazov, D. C. Higgins, C. Hahn, T. F. Jaramillo, *Nat. Catal.* **2019**, *2*, 702 – 708.
[25] A. Auer, M. Andersen, E.-M. Wernig, N. G. Hörmann, N. Buller, K. Reuter, J. Kunze-Liebhäuser, *Nat. Catal.* **2020**, *3*, 797—803.
[26] C. Choi, S. Kwon, T. Cheng, M. Xu, P. Tieu, C. Lee, J. Cai, H. M. Lee, X. Pan, X. Duan, W. A. Goddard, Y. Huang, *Nat. Catal.* **2020**, *3*, 804—812 .
[27] T. Kim, G. T. R. Palmore, *Nat. Commun.* **2020**, *11*, 3622.
[28] H. Jiang, Z. Hou, Y. Luo, *Angew. Chem. Int. Ed.* **2017**, *56*, 15617 – 15621; *Angew. Chem.* **2017**, *129*, 15823 – 15827.
[29] M. Liu, Y. Pang, B. Zhang, P. De Luna, O. Voznyy, J. Xu, X. Zheng, C. T. Dinh, F. Fan, C. Cao, F. P. de Arquer, T. S. Safaei, A. Mepham, A. Klinkova, E. Kumacheva, T. Filleter, D. Sinton, S. O. Kelley, E. H. Sargent, *Nature* **2016**, *537*, 382 – 386.
[30] Q.-X. Chen, Y.-H. Liu, X.-Z. Qi, J.-W. Liu, H.-J. Jiang, J.-L. Wang, Z. He, X.-F. Ren, Z.-H. Hou, S.-H. Yu, *J. Am. Chem. Soc.* **2019**, *141*, 10729 – 10735.
[31] R. Subbaraman, D. Tripkovic, D. Strmcnik, K.-C. Chang, M. Uchimura, A. P. Paulikas, V. Stamenkovic, N. M. Markovic, *Science* **2011**, *334*, 1256 – 1260.
[32] S. Sharifi-Asl, D. D. Macdonald, *J. Electrochem. Soc.* **2013**, *160*, H382 – H391.
[33] E. Liu, J. Li, L. Jiao, H. T. T. Doan, Z. Liu, Z. Zhao, Y. Huang, K. M. Abraham, S. Mukerjee, Q. Jia, *J. Am. Chem. Soc.* **2019**, *141*, 3232 – 3239.
[34] J. Li, X. Li, C. M. Gunathunge, M. M. Waegele, *Proc. Natl. Acad. Sci. USA* **2019**, *116*, 9220 – 9229.
[35] J. D. Roth, M. J. Weaver, *Langmuir* **1992**, *8*, 1451 – 1458.
[36] H. Daiguji, *Chem. Soc. Rev.* **2010**, *39*, 901 – 911.

Manuscript received: December 9, 2020
Accepted manuscript online: March 3, 2021
Version of record online: April 8, 2021

